Hindawi
Journal of Engineering
Volume 2024, Article ID 3280563, 19 pages
https://doi.org/10.1155/2024/3280563

Research Article

The Role of Wall Mechanics in the Hemodynamics of a Realistic Abdominal Aortic Aneurysm: A Fluid-Structure Interaction Study

Jafar Moradicheghamahi [1,2]

[1]*University of Bordeaux, Talence, Bordeaux, France*
[2]*Liryc-Electrophysiology and Heart Modeling Institute, Fondation Bordeaux Université, Pessac, Bordeaux, France*

Correspondence should be addressed to Jafar Moradicheghamahi; jafar.moradicheghamahi@urv.cat

Received 1 November 2023; Revised 19 February 2024; Accepted 7 April 2024; Published 25 April 2024

Academic Editor: Ran Zhao

Abdominal aortic aneurysm (AAA) can lead to high mortality rates and further complications such as stroke or heart attack due to the risk of rupture and thrombosis. Wall mechanics play a crucial role in the development and progression of aneurysms. This study investigated the effects of wall mechanics on hemodynamic parameters in AAA to understand the risk of rupture and thrombosis. The impact of three aortic wall models (rigid, linear elastic, and hyperelastic) on structural and hemodynamic parameters was examined using CFD and FSI techniques. The blood was modeled using the Carreau non-Newtonian model, and the flow was simulated using the k-ω model. Physiological pulses were used for the velocity at the inlet and the pressure at the outlet. The results demonstrated close similarity between the predictions of the linear elastic and hyperelastic models, in contrast to the somewhat different results of the rigid model. The hyperelastic model predicted higher deformation and von Mises stress levels than the elastic model, although the difference in stress predictions was smaller than the difference in deformation predictions. The rigid model evaluated the time-averaged wall shear stress and oscillatory shear index higher than the other two models in the aneurysmal area but with a lower relative residence time. In general, the hyperelastic model predicted a higher risk of rupture than linear elastic models and a higher risk of thrombus formation than the other two models. The rigid model had the most optimistic prediction.

1. Introduction

Abdominal aortic aneurysm (AAA) is one of the prevalent cardiovascular disorders in the circulatory system and is commonly found in the infrarenal segment of the abdominal aorta, between the renal arteries and the iliac bifurcation. Aneurysm refers to the permanent and irreversible dilation of the arterial walls during which the arterial wall experiences significant degradation in its materials. In an aneurysm, at least three different stages are distinguishable as follows: genesis, progression, and rupture. The exact initiation process is yet to be understood; however, it is reported that the degradation of elastin and significant loss of the media layer in its smooth muscle cell are the underlying processes observed in the initiation of the aneurysm [1, 2]. In other words, the media layer in an aneurysmatic arterial wall approximately vanishes and the arterial wall becomes thinner. Therefore, any factor contributing to the weakening of the arterial wall can trigger the aneurysm. During the progression, an aortic aneurysm reaches at least 1.5 times the healthy aorta in diameter and can swell to four times its initial diameter [3]. The current guideline for clinical intervention is the maximum transverse diameter of 50 to 55 mm [4]. However, rupture is seen in cases below this threshold, and patients with quite larger geometrical characteristics than the threshold are reported to experience no rupture during their lifetime [4].

Computational modeling has become a valuable approach for studying abdominal aortic aneurysm (AAA) due to its numerous advantages over traditional experimental and clinical studies [5]. Computational methods offer a unique opportunity to simulate and analyze complex

hemodynamic and structural processes occurring in the arterial wall and blood flow, providing insights into the mechanisms and pathophysiology of AAA [6]. Moreover, computational modeling allows for the evaluation of various wall mechanics and blood flow conditions, which are difficult to achieve in traditional studies [7]. Additionally, computational simulations can be conducted with reduced costs and time, without exposing patients to potential risks associated with invasive procedures or drug administration [8, 9].

In light of the critical role that advanced computational modeling plays in the analysis and treatment of cardiovascular disorders, particularly abdominal aortic aneurysm (AAA), recent research emphasizes the necessity of integrating state-of-the-art methodologies and findings. Innovative computational techniques, as detailed in recent studies, have shown promising advancements in simulating the hemodynamic effects of treatments and understanding the intricate dynamics within the aneurysm sac [10]. Moreover, these studies offer insights into optimizing treatment strategies through detailed analyses of stent design parameters, directly contributing to the precision and effectiveness of AAA interventions [11]. This integration of cutting-edge computational research underscores the potential for significant improvements in AAA management, highlighting the importance of incorporating these advancements into our study to advance the field further.

Blood is comprised of plasma, minerals, and red blood cells, and its viscosity decreases as the shear rate increases due to the shear-thinning behavior that is attributed to the deformation of red blood cells in the flow. Several studies have been conducted in recent years to establish an appropriate model for blood fluid behavior, with a focus on examining the WSS-dependent parameters for different rheological models [12, 13]. These investigations have revealed that the Carreau non-Newtonian model is better at predicting these parameters. Therefore, the Carreau model has been suggested as the most suitable model for blood in various studies [7, 14] and will also be used in this study.

In the complex domain of cardiovascular studies, particularly in examining abdominal aortic aneurysms (AAAs), the accurate simulation of flow phenomena becomes paramount. The determination of a turbulent flow regime within the AAA leverages the unique geometric characteristics and pulsatile nature of blood flow inherent to this condition. In particular, the dilation and irregular shapes common to AAAs foster conditions conducive to flow separation, recirculation, and vortex shedding, underscoring the necessity of employing turbulence models to simulate the intricate hemodynamics accurately [15]. These phenomena, emblematic of turbulent flows, alongside the pulsatile flow's variable velocities and directions, substantiate the turbulent nature of blood flow within AAAs, thereby making turbulence modeling an indispensable tool in these simulations [16, 17]. Among the various turbulence models available, the k-omega (k-ω) model is distinguished by its adeptness at capturing boundary layer phenomena and its efficiency in integrating into the viscous sublayer without requiring additional damping functions. This capability renders the k-ω model particularly advantageous for cardiovascular applications, where a granular understanding of near-wall flow behavior exerts a significant influence on wall shear stress distributions and subsequent biological responses [13, 18–20]. The choice of the k-ω model over others, such as the k-epsilon (k-ε), is informed by its demonstrated precision in depicting near-wall turbulence—a critical aspect in cardiovascular flows, including those altered by AAA. This model's preference in computational studies on AAA and other cardiovascular conditions is further justified by its role in enhancing the interaction between blood components and endothelial cells, thereby facilitating platelet activation and the accumulation of blood lipids in the intima [21, 22], linking turbulent flow characteristics directly to the processes contributing to thrombosis formation [23].

Structural parameters such as deformation of the artery wall and von Mises stress are critical in evaluating the rupture risk of abdominal aortic aneurysm (AAA) in computational studies. High deformation and von Mises stress can lead to mechanical failure and rupture [24, 25]. Several studies have demonstrated a significant correlation between these structural parameters and an increased risk of rupture [26–29]. However, the choice of model for the aortic wall, whether a linear elastic or hyperelastic model, can significantly affect the evaluation of rupture risk in computational studies of AAA [30]. Hyperelastic models can better capture the nonlinear behavior of the arterial wall and have been shown to lead to more accurate predictions of rupture risk compared with linear elastic models [25, 31]. Hyperelastic models generally predict higher deformation and von Mises stress values than linear elastic models, especially for larger aneurysms and higher pressures. Overall, hyperelastic models may provide a more accurate prediction of rupture risk in AAA [32, 33].

Thrombosis is a common complication associated with AAA, with a reported prevalence ranging from up to 70% depending on the aneurysm's size and location. It can lead to blockage of the aneurysm sac and cause ischemia or embolization. To assess the risk of thrombosis occurrence in AAA, three hemodynamic parameters that depend on wall shear stress (WSS) are useful, including time-averaged WSS (TAWSS), the oscillating shear index (OSI), and the relative residence time (RRT). Low and high TAWSS values, as well as high OSI values, indicate an increased risk of thrombus formation, whereas high RRT values indicate stagnant flow that can contribute to thrombosis. The choice of wall mechanics model can affect the evaluation of thrombosis risk in AAA using hemodynamic parameters. Rigid wall models tend to overestimate WSS and provide inaccurate predictions of hemodynamic parameters, while elastic and hyperelastic models better capture complex wall motion, leading to more accurate predictions of hemodynamic parameters and thrombosis risk [34, 35]. The choice of wall mechanics model should be considered carefully when assessing thrombosis risk in AAA using hemodynamic parameters [25, 36].

Prior research in the domain of abdominal aortic aneurysm (AAA) has often relied on both rigid and elastic wall models, with many studies introducing simplifications in

aspects such as geometry, flow dynamics, or material characteristics. These simplifications have historically constrained the depth of understanding attainable regarding the predictive accuracy of these models for rupture and thrombosis risks under conditions that closely mimic clinical realities. In addressing this gap, this study advances the field by employing a comprehensive approach that integrates a realistic AAA geometry, the k-omega turbulent flow model, the Carreau model for non-Newtonian blood behavior, and physiological pulse simulations as boundary conditions. This methodological rigor enabled a nuanced comparison between rigid and elastic wall models, elucidating their respective impacts on structural integrity and hemodynamic factors critical to assessing rupture and thrombosis risks. Significantly, the findings of the present study not only challenge simplifying modeling assumptions but also help achieve more accurate, personalized diagnostic and therapeutic strategies in cardiovascular care. By bridging these methodological divides, this study contributes a pivotal resource for future research and clinical practice, underscoring the critical role of sophisticated simulation techniques in enhancing our understanding and management of AAA.

2. Methodology

2.1. Governing Equations. The general form of the incompressible unsteady Reynolds-averaged Navier–Stokes equations, which are used to determine fluid motion, is as follows [20, 37, 38]:

$$\frac{\partial \rho}{\partial t} + \frac{\partial}{\partial x_i}(\rho u_i) = 0, \tag{1}$$

$$\frac{\partial}{\partial t}(\rho u_i) + \frac{\partial}{\partial x_j}\left(\rho u_i u_j\right) = -\frac{\partial p}{\partial x_i} + \frac{\partial}{\partial x_j}\left[\mu\left(\frac{\partial u_i}{\partial x_j} + \frac{\partial u_j}{\partial x_i} - \frac{2}{3}\delta_{ij}\frac{\partial u_k}{\partial x_k}\right)\right] + \frac{\partial}{\partial x_j}\left(-\rho\overline{u_i' u_j'}\right) + F_i. \tag{2}$$

For laminar flows, the term $\partial/\partial x_j(-\rho\overline{u_i' u_j'})$ in (2) is excluded. However, for turbulent flows, this term is modeled as follows:

$$\mu_t S^2 = -\rho\overline{u_i' u_j'}\frac{\partial u_j}{\partial x_i} \text{ with } S = \sqrt{2S_{ij}S_{ij}}, \tag{3}$$

where S denotes the modulus of the mean strain rate tensor, μ_t represents the turbulence viscosity of blood, and ρ refers to the density. The determination of μ_t in the k-ω turbulence model used for this study is expressed as follows:

$$\mu_t = \alpha^* \frac{\rho k}{\omega}. \tag{4}$$

The correction for the low Reynolds number is triggered by the coefficient α^*, which functions to dampen turbulent viscosity [37]. The values of k and ω are computed by the following equations, respectively.

$$\frac{\partial}{\partial t}(\rho k) + \frac{\partial}{\partial x_i}(\rho k u_i) = \frac{\partial}{\partial x_j}\left[\left(\mu + \frac{\mu_t}{\sigma_k}\right)\frac{\partial k}{\partial x_j}\right] + G_k - Y_k + S_k, \tag{5}$$

$$\frac{\partial}{\partial t}(\rho \omega) + \frac{\partial}{\partial x_i}(\rho \omega u_i) = \frac{\partial}{\partial x_j}\left[\left(\mu + \frac{\mu_t}{\sigma_\omega}\right)\frac{\partial \omega}{\partial x_j}\right] + G_\omega - Y_\omega + S_\omega. \tag{6}$$

Reference [37] provides the constants and parameters used in (4)–(6).

The typical approach to describe the mechanical characteristics of the artery wall is to use the solid elastodynamic momentum equation (39):

$$\rho_s \ddot{u}_s = \nabla_0 \cdot \sigma_s + \rho_s f. \tag{7}$$

In the equation, u_s refers to the vector indicating the displacement of the solid, σ_s represents the Cauchy stress tensor, f is the vector representing external forces exerted on the solid, and ρ_s is the volumetric mass of the solid.

2.2. Problem Statement. The present study involves a fluid-structure interaction (FSI) analysis of an aneurysmal aorta using a realistic geometry obtained from CT scan data. The primary objective of this research is to investigate the impact of different models for the artery wall on structural and hemodynamic parameters. The three models under consideration for the artery wall are solid, linear elastic, and hyperelastic.

The fluid and solid domains' geometries are depicted in Figure 1.

Physiological pulses were employed at the inlet and the outlet to create realistic boundary conditions, and the inlet velocity pulse and the outlet pressure pulse are illustrated in Figures 2(a) and 2(b), respectively [40, 41].

The solid model was investigated using a computational fluid dynamics (CFD) study, whereas FSI studies were used for the elastic and hyperelastic models. This study assesses the performance of different wall models and compares their impact on the structural and hemodynamic parameters, which are vital for the proper diagnosis and treatment of aneurysmal aorta.

The analysis and visualization of flow were carried out using the ANSYS Fluent 2020 R1 commercial CFD software. The third-order MUSCL differencing scheme was employed for discretizing the equations. The pressure-velocity correction method was coupled to the simulations. A residual error convergence threshold of $1e-6$ was set for the momentum equations. To ensure reliable results and eliminate transient effects, unsteady simulations were conducted for three consecutive pulses as recommended in prior investigations [42], and the outcome was based on the third pulse. The maximum number of iterations per step was fixed at 40 for all simulations, while the time step was 0.005 seconds. Furthermore, in sensitivity testing, no significant alterations were observed while using a time step of 0.002 and maximum iterations of 80.

2.3. Material Properties. The density of the blood was $\rho = 1060\ \text{kg/m}^3$, and the Carreau non-Newtonian model was employed in this simulation. The Carreau model equation is used to predict the non-Newtonian behavior of blood, and it can be expressed as follows [43, 44]:

$$\mu = \mu_\infty + (\mu_0 - \mu_\infty)\left(1 + A|\dot{\gamma}|^2\right)^n, \tag{8}$$

where the values of A, n, μ_∞, and μ_∞ are 10.976, −0.3216, 0.0035, and 0.056, respectively.

The AAA wall is assumed to be a nonlinear, isotropic, hyperelastic material with a density of $2200\ \text{kg/m}^3$, Young's modulus $E = 2.7$ MPa, and Poisson's ratio $\upsilon = 0.45$. For hyperelastic materials, the strain-energy function based on the Mooney–Rivlin material model is given as follows:

$$W = \alpha(I_B - 3) + \beta(I_B - 3)^2, \tag{9}$$

where W is the strain-energy density, B is the left Cauchy–Green tensor, and I_B is the first invariant of B; and α and β are the model parameters indicative of the mechanical properties of the aneurysmal wall. The material parameters

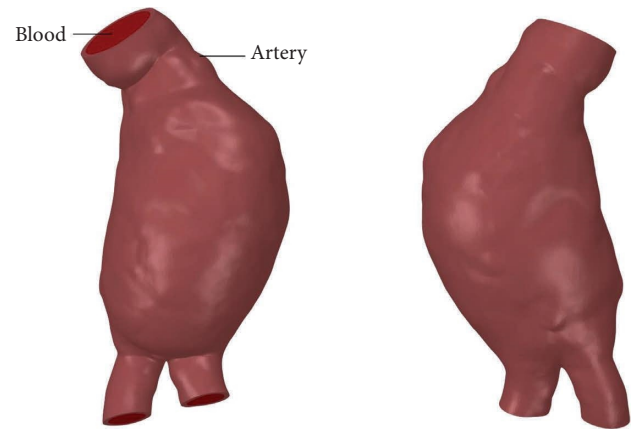

Figure 1: Used geometry in the simulations.

$\alpha = 17.4\ \text{N/cm}^2$ and $\beta = 188.1\ \text{N/cm}^2$ are based on the means of the best-fit material parameters of the data examined by Raghavan and Vorp [45]. The bulk modulus (κ_{MR}) for the Mooney–Rivlin model is determined as follows:

$$\kappa_{\text{MR}} = \frac{E}{3(1-2\upsilon)}. \tag{10}$$

2.4. Mesh Study. A simulation was conducted using four different meshes containing elements of varying sizes, to verify that the outcomes were not affected by the quantity of computational cells. Table 1 provides details on all the meshes used in the study.

The Carreau model was used as the blood non-Newtonian model, and the k-ω model was used as the turbulent model for this steady-state simulation. The velocity and pressure at the time of the pressure peak were used, with an inlet flow rate of $6.4e-5\ \text{m}^3/\text{s}$ and an outlet pressure of 123 mmHg. The mean values of the wall shear stress (WSS) were calculated along the z direction and compared for different meshes in Figure 3. The figure shows that there was no change in the mean WSS even after increasing the number of cells from 263,766 to 349,681. Based on the mesh study, a mesh with a minimum cell length of 0.0008 m, a maximum cell length of 0.0016 m, and a total cell number of 263,766 were selected, as shown in Table 1. Polyhedral and hexagonal elements were used in this research, and the final mesh details are shown in Figure 4.

The artery wall underwent a similar mesh study, employing the von Mises stress parameter. Ultimately, a mesh consisting of 295823 total elements with an element size of $8e-4$ was chosen. Figure 5 depicts the details of this mesh.

2.5. Hemodynamic Parameters. In this study, three hemodynamic parameters that are commonly used in the study of thrombosis and atherosclerosis [46] were used to investigate the mechanics of the artery wall. These parameters are based on wall shear stress (WSS) and include time-averaged WSS (TAWSS), oscillating shear index (OSI), and relative residence time (RRT).

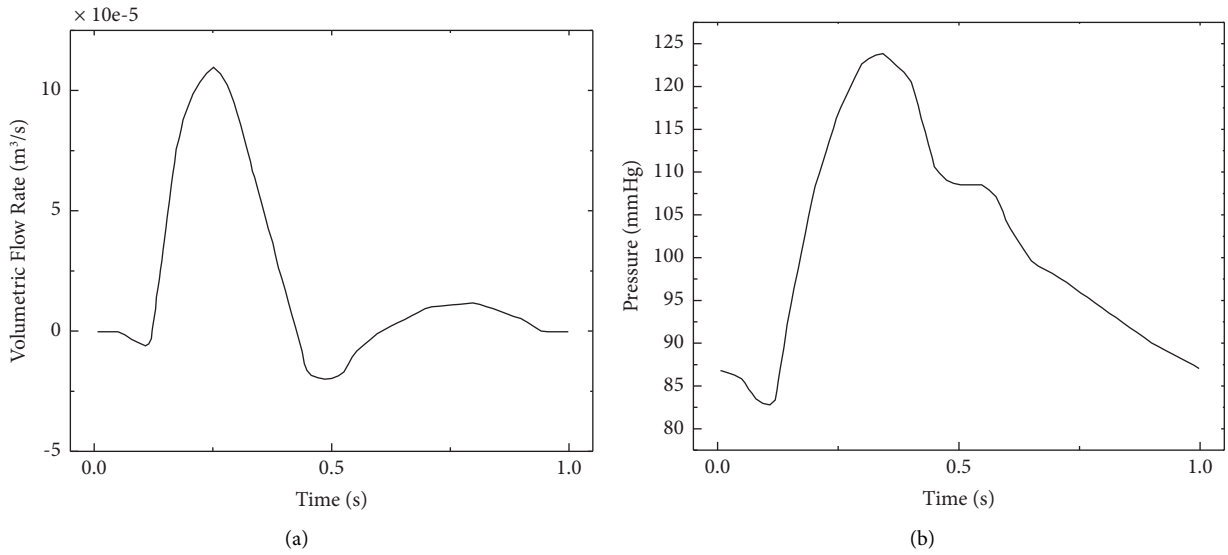

Figure 2: Used pulses as inlet (a) and outlet (b) boundary conditions [40, 41].

Table 1: Characteristics of the investigated meshes in the mesh study.

Case number	Minimum cell length	Maximum cell length	Number of cells
1	0.002	0.004	41641
2	0.001	0.002	166516
3	0.0008	0.0016	263766
4	0.0007	0.0014	349681

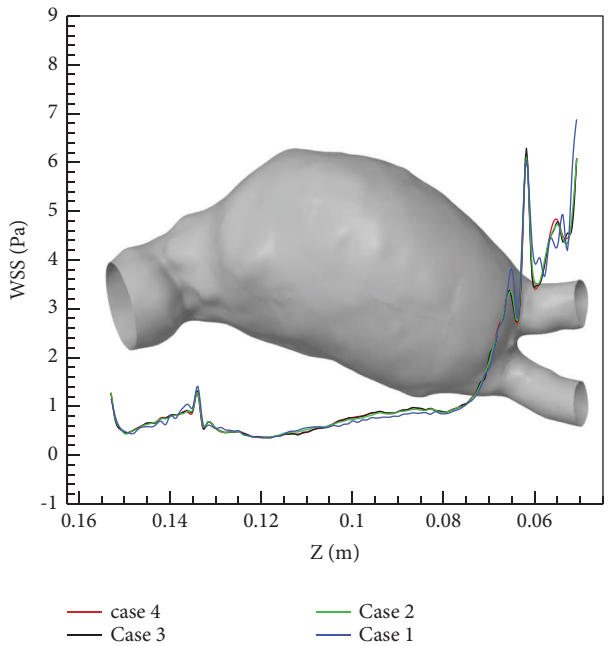

Figure 3: Mesh independence study; averaged WSS changes along the z direction for meshes with different element sizes.

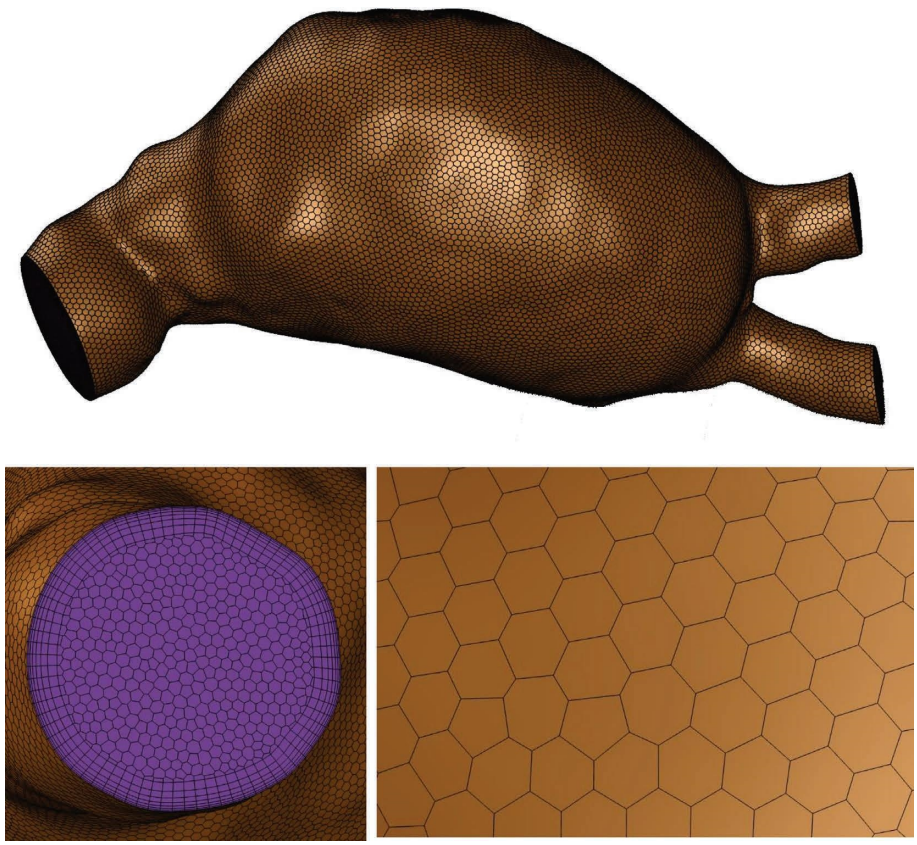

Figure 4: Details of the selected mesh for the fluid domain.

Earlier studies [47, 48] have used the following equation to calculate the TAWSS variable, which is used to determine the total shear stress on the artery wall throughout the entire cardiac cycle.

$$\mathrm{TAWSS} = \frac{1}{T}\int_0^T \left|\tau_s\right| \mathrm{dt}. \tag{11}$$

During a cardiac cycle, endothelial cells are constantly exposed to varying shear stresses. The oscillating shear index (OSI) is a measure used to quantify these cyclic fluctuations. It provides insight into the average duration of flow separation and reattachment [49]. Larger OSI values indicate regions where flow direction changes more frequently, whereas smaller values are associated with a lack of WSS cyclic variations [50]. The OSI value ranges from zero for pure unidirectional flows to 0.5 for entirely oscillatory flows [51]. For pure pulsatile flows, the OSI can be calculated using the following formula [52, 53]:

$$\mathrm{OSI} = \frac{1}{2}\left(1 - \frac{\left|1/T\int_0^T \tau_s \,\mathrm{dt}\right|}{1/T\int_0^T \left|\tau_s\right| \mathrm{dt}}\right). \tag{12}$$

The distribution of frictional forces on the inner surface of the artery is evaluated by the relative residence time (RRT) parameter. An area with high RRT is subjected to both low and oscillating wall shear stresses simultaneously [54]. RRT is a measure of how closely the particles remain in proximity to the wall and can be calculated using the following formula [55]:

$$\mathrm{RRT} = \frac{1}{(1 - 2\,\mathrm{OSI}) \cdot \mathrm{TAWSS}}. \tag{13}$$

3. Results and Discussion

3.1. Deformation. Geometrical changes in the aneurysmal wall are significant and they cause considerable changes in the mechanics of the wall, which could lead to rupture. During one cardiac cycle, blood flows through the abdominal aorta, causing deformation of the aneurysmal aorta. The deformation of the aorta during a cardiac cycle is a complex process that is influenced by the pulsatile flow of blood, the elasticity of the arterial wall, and the geometry of the aorta. Understanding the deformation of the aneurysmal aorta during one cycle is important for assessing the risk of rupture and designing effective treatment strategies. In this research, the structural parameters, including deformation and von Mises stress, are investigated by presenting the contours of these parameters at the systolic peak of the pressure wave during the cardiac cycle.

The deformation contours for both linear elastic and hyperelastic models are shown in Figure 6. These contours correspond to the peak systolic pressure time. Due to the

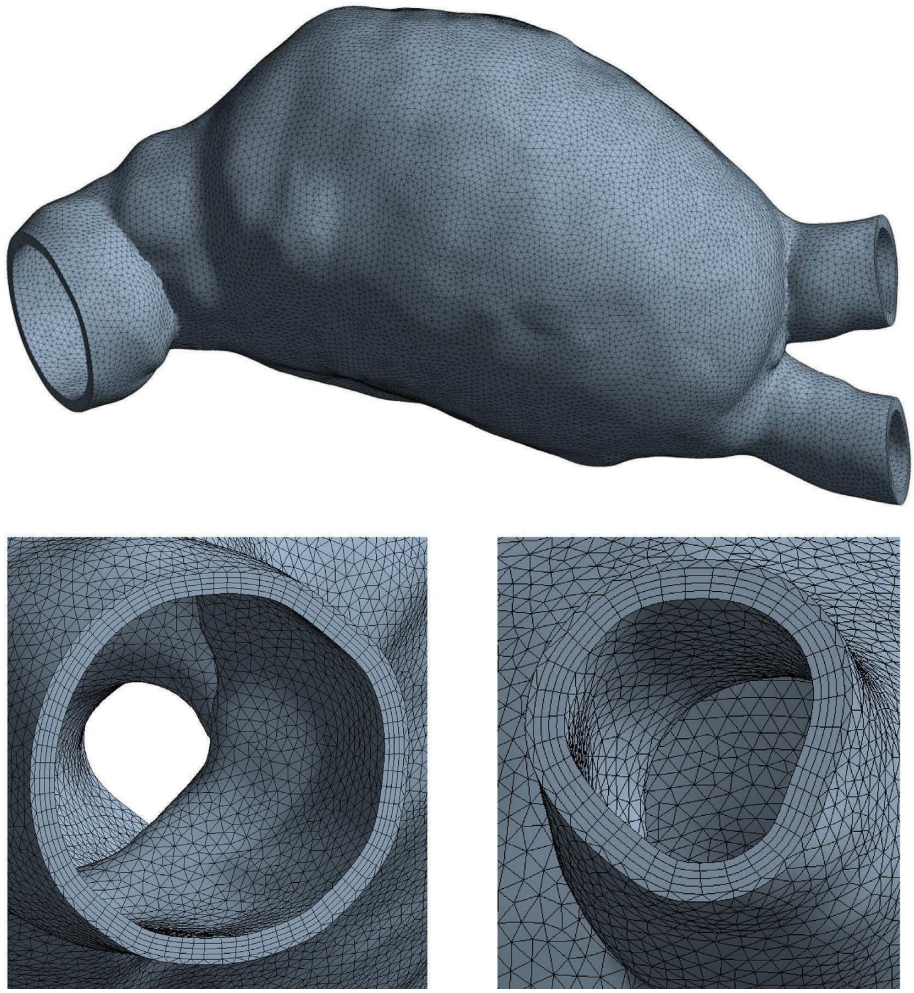

Figure 5: Details of the selected mesh for the solid domain.

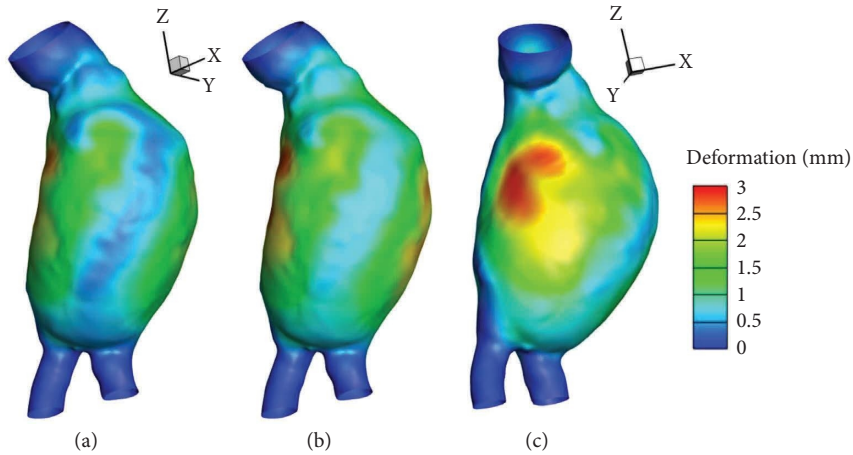

Figure 6: Deformation of the aneurysmal wall at the systolic peak of the pressure wave; (a) the deformation predicted by the elastic model; (b) and (c) the deformation predicted by the hyperelastic model for two different views.

increase in pressure resulting from the increase in the cross-sectional area of the flow, the deformation level is higher in the area affected by the aneurysm. In addition, the difference in the prediction of deformation level by these two models is shown in Figure 7 for three different views. As can be seen in Figure 7, the hyperelastic model predicts slightly higher deformation levels than the linear elastic model. The highest deformation level is related to a relatively small area in the

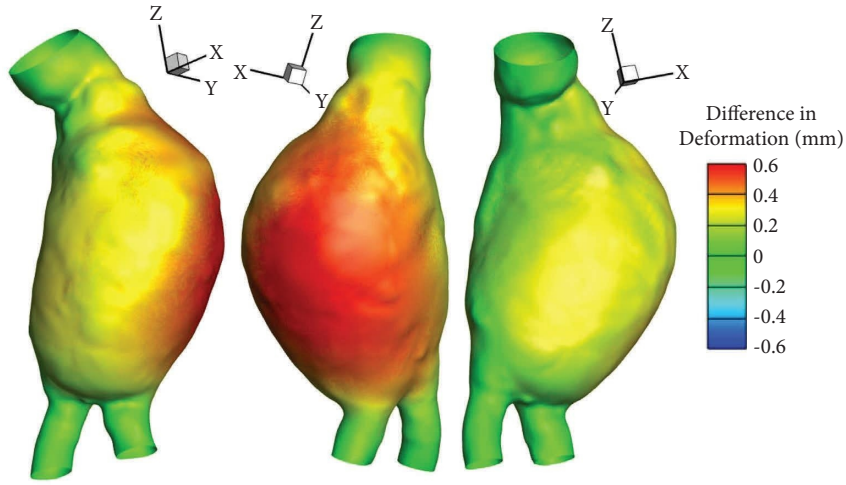

Figure 7: Difference in deformation contours between hyperelastic and linear elastic models.

upper half of the lumen. The greatest difference between the two models is near the other side of the aortic wall and is about 0.6 mm. The difference between the two models in the area with the highest deformation is less than 0.2 mm.

To better understand the difference between the two models in predicting deformation, the average deformation in the z direction is shown in Figure 8(a). In addition, the difference between the mean predicted deformation by the two models is presented in Figure 8(b). As observed, the greatest difference between the two models in predicting the average deformation is about 0.33 mm, which seems negligible compared with the diameter of the aorta in this region.

Understanding the deformation of the aneurysm during one cycle can help identify regions of the aneurysm that are particularly prone to rupture. For example, if certain areas of the aneurysm are subjected to higher levels of stress or strain during one cycle, they may be more likely to rupture in the future [49]. By identifying these regions, clinicians can develop more targeted treatment strategies to reduce the risk of rupture [50]. Figures 6 and 7 reveal that the wall deformation within the lumen of the aorta is greater than that in other regions, resulting in an evident increase in the risk of rupture. Additionally, a dilated section that has a higher intensity of aneurysm exhibits greater deformation, leading to a consequent increase in the risk of rupture. Moreover, the hyperelastic model predicts a higher deformation than the linear elastic model. This issue has also been observed in previous research studies [56]. This not only results in predicting a higher risk of rupture but also leads to differences in predicting other parameters based on wall shear stress, which are used in the analysis of thrombotic areas. The level of deformation is high on both sides of the wall, but due to the smaller area on the right side of the wall, there is likely a higher risk of rupture in this area. To obtain a more precise understanding, it is necessary to analyze the von Mises stress in this region.

3.2. Von Mises Stress. Von Mises stress is an important factor to consider in the evaluation and management of aortic aneurysms. By providing a more comprehensive understanding of the stress levels in the aortic wall, it can help guide treatment decisions and improve outcomes for patients with this condition.

Figure 9 displays the distribution of von Mises stress at various points on the artery wall during the peak pressure. The difference between the two models (i.e., hyperelastic and linear elastic) in terms of von Mises stress is shown in Figure 10. Stress in the aneurysmal region is higher than that in healthy areas, and points with high stress values are more prominent in the upper half of the aneurysm. As expected, the location that experienced the highest deformation also has the highest von Mises stress. Similar to the deformation parameter, hyperelastic models predict slightly higher von Mises stress than linear elastic models. Another notable point is that both models have almost the same prediction for the critical point locations.

The graphs in Figure 11 provide a clearer understanding of the difference between the two models in predicting the von Mises stress parameter. These graphs show the average value of von Mises stress on the aortic wall along the Z-axis. Additionally, the difference between the two models at different points is also shown in Figure 11(b). As can be seen, the difference between the two models in predicting stress values is lower than their difference in predicting deformation values.

Studies have shown that von Mises stress is a useful predictor of the risk of rupture in aortic aneurysms, with significantly higher levels found in ruptured aneurysms than in nonruptured ones [50]. As such, von Mises stress is a critical metric for identifying aneurysms that are at high risk of rupture, and its analysis can help clinicians make informed decisions about the best course of treatment. High von Mises stress levels may suggest that the aneurysm requires more aggressive treatment, such as surgery or

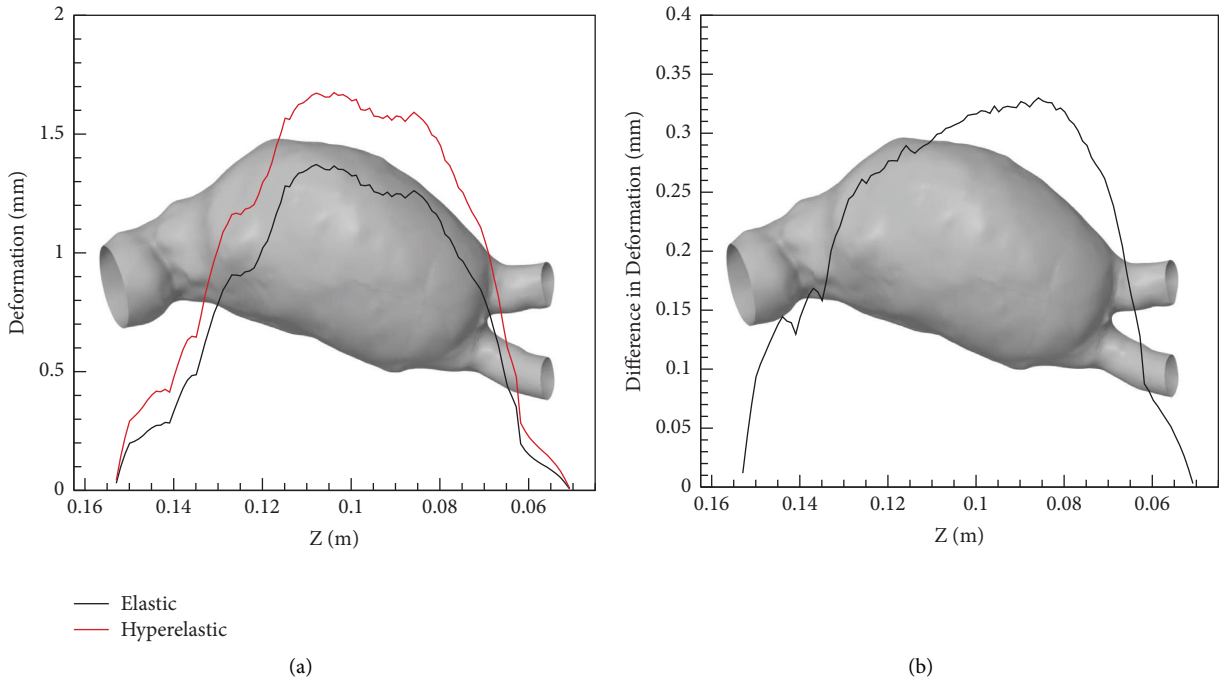

FIGURE 8: Comparison of linear elastic and hyperelastic models in predicting average deformation along z direction; (a) average deformation for each model; (b) difference in models' predictions.

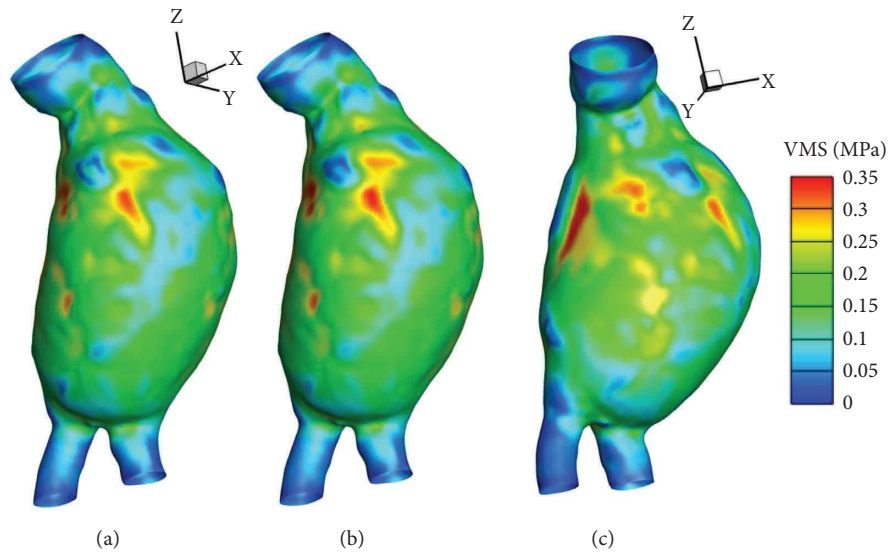

FIGURE 9: Distribution of von Mises stress on the aneurysmal wall at the systolic peak of the pressure wave; (a) the elastic model; (b) and (c) the hyperelastic model.

endovascular repair, while lower levels may indicate that conservative management is more appropriate [57]. Therefore, von Mises stress analysis can guide treatment decisions for aortic aneurysms. As can be observed in Figures 9 and 10, the von Mises stress in the right wall of the aorta is significantly higher in a small area than at other points. In the deformation analysis section, it was observed that this area has a high deformation despite its small surface area. Therefore, this area can be considered the most susceptible point for aortic rupture. The predicted von Mises stress levels in both models are close to each other, although the hyperelastic model predicts slightly higher von Mises stress levels. Another notable point that has been emphasized in previous studies is the high average von Mises stress in the location where the aneurysm severity is higher.

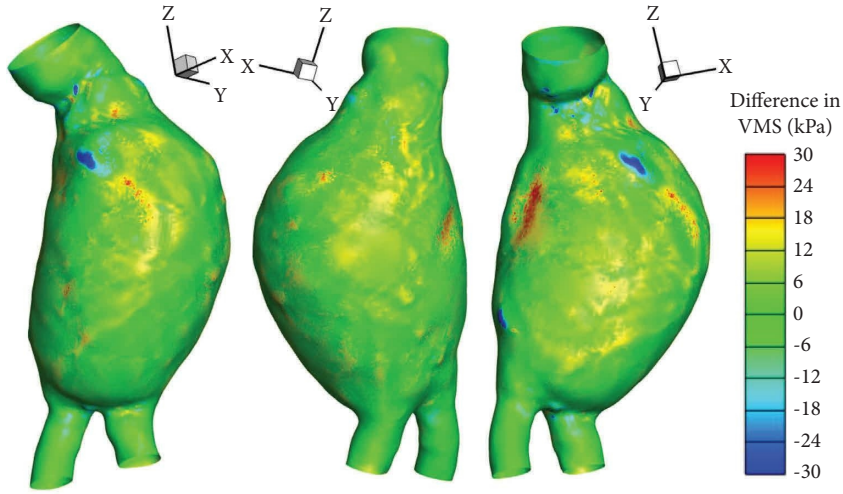

Figure 10: Difference in von Mises stress contours between hyperelastic and linear elastic models.

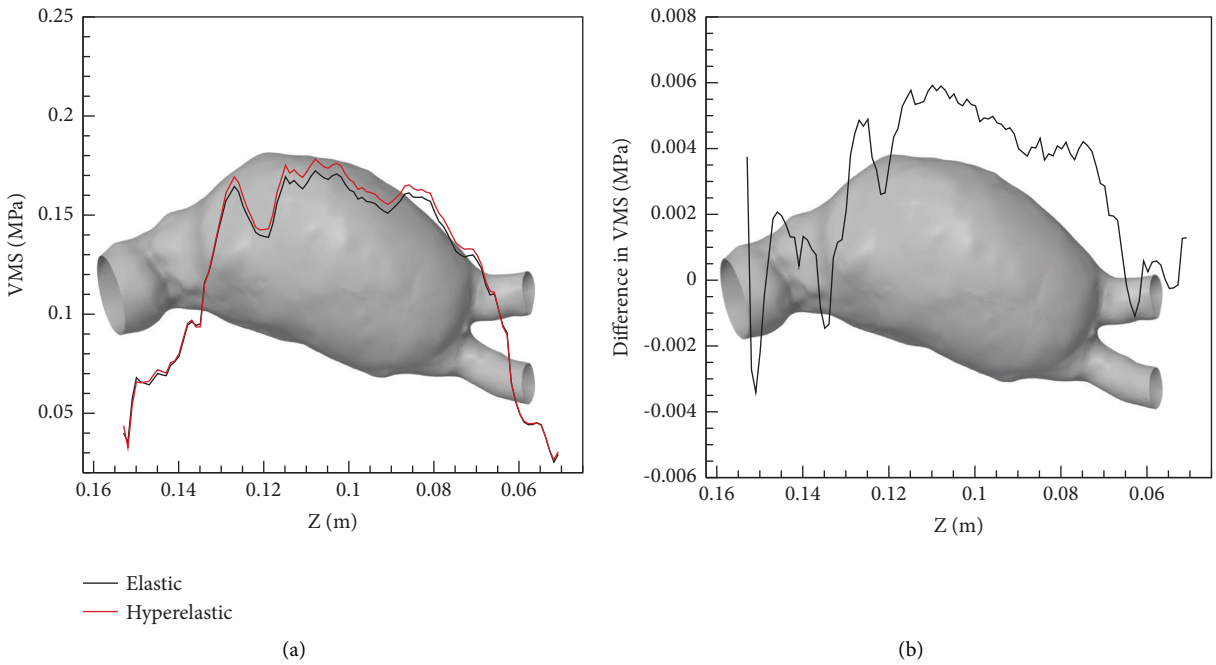

Figure 11: Comparison of linear elastic and hyperelastic models in predicting average von Mises stress along z direction; (a) average VMS for each model; (b) difference in models' predictions.

3.3. Time-Averaged Wall Shear Stress (TAWSS). Aneurysms occur when the arterial wall weakens and distends, causing a bulge or sac that protrudes from the normal arterial wall. This can alter the blood flow pattern and result in changes in wall shear stress (WSS) values. In particular, WSS in aneurysms tends to be lower than that in healthy arterial segments, indicating that the arterial wall is exposed to lower levels of shear stress [56].

In Figure 12, the TAWSS contours obtained from all three presented models are shown. Additionally, Figure 13 illustrates the differences between these models in predicting TAWSS values. As can be seen, the level of stress is very low in the region affected by the aneurysm. These low shear stress values are due to the sudden increase in cross-sectional area and the decrease in mean velocity in this region. Also, the presence of points with high shear stress at the iliac bifurcation is noteworthy. The reason for the high shear stress in this location may be the increase in pressure in the aneurysm sac, which leads to an increase in flow velocity in the region after it. By examining Figures 12 and 13, it is not possible to clearly determine which model predicts the shear stress in the aneurysm-affected region to be lower or higher. A notable point from this figure is that the linear elastic and hyperelastic models predict almost the same level of stress in the average time.

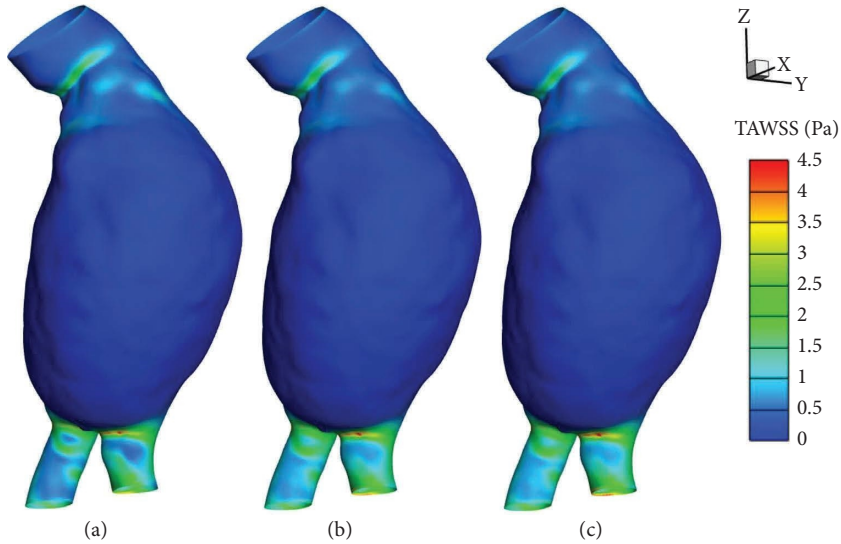

FIGURE 12: TAWSS contours on the aortic wall for different models; (a) rigid wall model; (b) linear elastic wall model; (c) hyperelastic wall model.

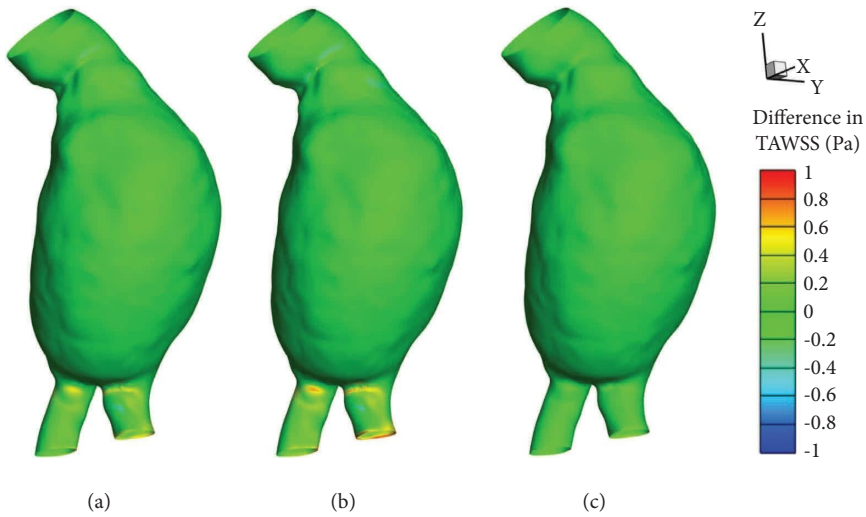

FIGURE 13: Difference in TAWSS contours on the aortic wall between different models; (a) $TAWSS_{elastic}$ - $TAWSS_{rigid}$; (b) $TAWSS_{hyperelastic}$ - $TAWSS_{rigid}$; (c): $TAWSS_{hyperelastic}$ - $TAWSS_{elastic}$.

To further investigate the impact of different models of arterial walls on TAWSS values in different regions, 2D graphs in Figure 14 showing the average values of this parameter along the *Z*-axis were used. As observed, both linear elastic and hyperelastic models had nearly identical predictions for TAWSS. However, in the region with very low shear stress, the rigid wall model predicted higher shear stress values than the other two models, while in points with high shear stress, the shear stress values calculated by linear elastic and hyperelastic models were higher.

Low wall shear stress (WSS) can lead to thrombus formation, endothelial cell dysfunction and damage, and low oxygen tension. Platelets can adhere to the endothelial cells lining the vessel wall, leading to the formation of a platelet-rich thrombus [58]. Low WSS can cause endothelial cells to produce less nitric oxide and upregulate pro-inflammatory cytokines and adhesion molecules, promoting platelet aggregation and thrombus formation [59]. Additionally, low WSS can create areas of low oxygen tension, resulting in the release of more adenosine diphosphate (ADP) from red blood cells, which is a potent activator of platelets [60]. Therefore, as seen in Figures 12 and 13, the magnitude of shear stress in the region most affected by the aneurysm is much lower than that in other areas, indicating the susceptibility of this area to thrombus formation. The rigid wall model predicts higher shear stress in this area than linear elastic and hyperelastic models, which means a lower risk of thrombus formation in this area. Another notable finding in these results is the good agreement between the linear elastic and hyperelastic models in predicting the risk of thrombus formation, although the linear elastic model has a slightly more optimistic prediction than the hyperelastic models.

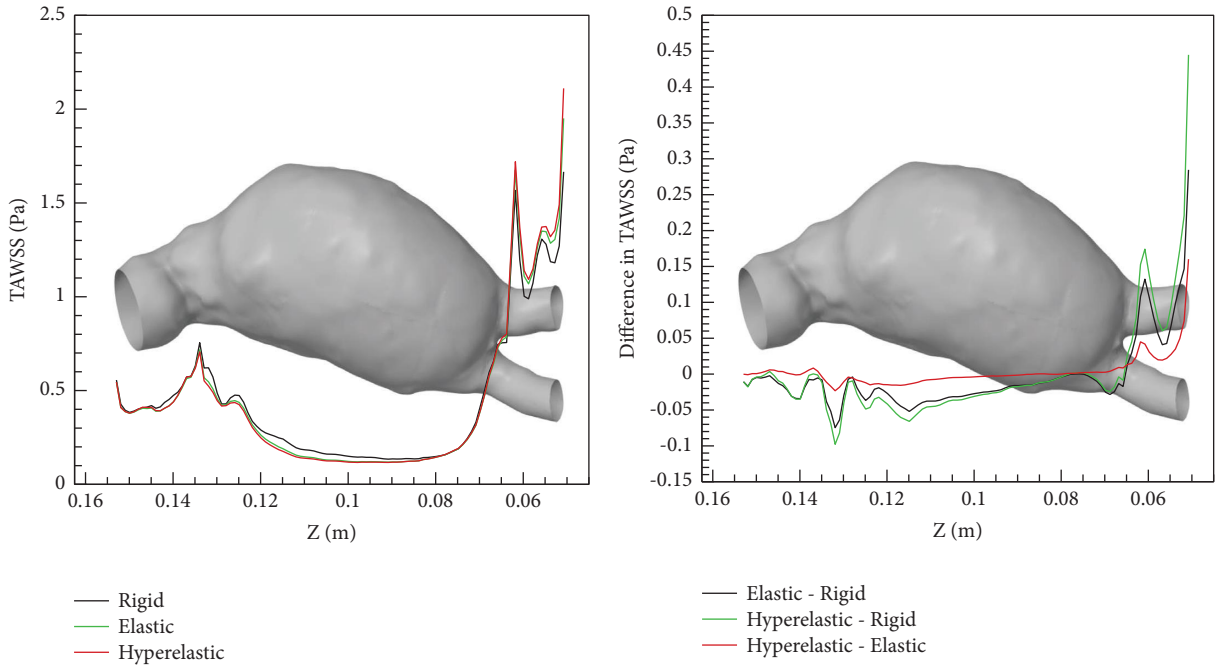

Figure 14: Comparison of different models in predicting average TAWSS along z direction; (a) average TAWSS for each model; (b) difference in models' predictions.

However, it should be noted that low shear stress alone does not necessarily lead to the identification of a thrombosis area, and it depends on the amount of shear stress oscillations at that point [61].

However, high WSS can have adverse effects, such as causing damage to endothelial cells that line the arterial wall. This is due to the creation of regions with high shear stress along the arterial wall. As a result, inflammation and further weakening of the arterial wall can occur [62]. Additionally, high WSS values can change blood flow patterns, potentially leading to aneurysm growth and rupture. For instance, vortex flows may form within the aneurysm sac, contributing to thrombus formation and further weakening of the arterial wall [63]. Based on what is observable in Figures 12 and 13, high shear stresses are present in two identifiable regions. The first region is located before the lumen, where the difference in shear stress predicted by all three models is not significant. However, in the second region, located at the iliac bifurcation, the solid wall model predicts lower levels of shear stress than the other two models, thus having a more optimistic prediction. Furthermore, the hyperelastic model predicts a higher risk of high shear stress in this region than the linear elastic model.

3.4. Oscillatory Shear Index (OSI). The oscillatory shear index (OSI) is a hemodynamic parameter that measures the magnitude of the oscillations in shear stress that occur during the cardiac cycle. High OSI values have been associated with the development and progression of aneurysms and can lead to the activation of mechanosensitive signaling pathways within the endothelial cells that line the arterial wall [64].

Figure 15 displays the predicted values of OSI by all three wall models at different locations along the artery. Figure 16 shows the differences among the models in evaluating the magnitude of shear stress fluctuations. Three locations with high OSI values are observed. The first location is before the onset of the aneurysm, which can be justified by the high curvature of the artery and changes in the direction of these fluctuations in shear stress. The second location is at the bottom of the aneurysm sac, where the flow is stagnant and rotational, and points with high OSI values can be predicted. The third location is after the bifurcation of the iliac, where the increase in velocity and turbulence leads to high OSI values. In contrast to TAWSS, the predicted 3D contours of OSI by the rigid wall model differ from the other two models. In the rigid wall model, a larger area is affected by oscillatory shear stress, while in the linear elastic and hyperelastic models, points with high shear stress fluctuations are concentrated at two points. Similar to the previous parameters, the linear elastic and hyperelastic models have almost similar predictions for the OSI parameter, despite a slight difference in the location of maximum shear stress fluctuations in the aneurysm sac.

Figure 17 shows the average value of the OSI parameter along the Z-axis. As can be seen, the average OSI predicted by the solid wall model is higher than the average predicted by the other two models at the location of the aneurysm sac. However, in the location of the iliac bifurcation, this model

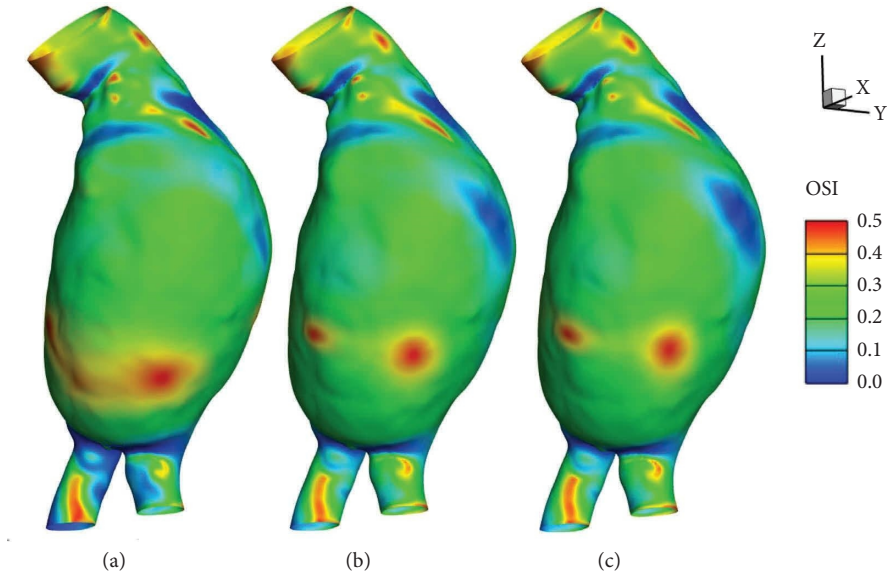

Figure 15: OSI contours on the aortic wall for different models; (a) rigid wall model; (b) linear elastic wall model; (c) hyperelastic wall model.

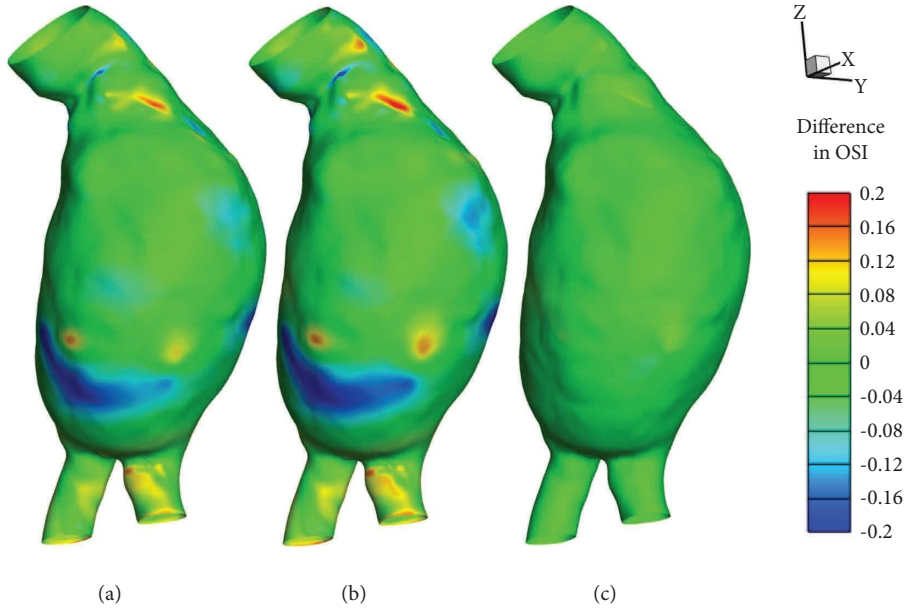

Figure 16: Difference in OSI contours on the aortic wall between different models; (a) $OSI_{elastic}$ - OSI_{rigid}; (b) $OSI_{hyperelastic}$ - OSI_{rigid}; (c) $OSI_{hyperelastic}$ - $OSI_{elastic}$.

predicts fewer oscillations in shear stress compared with the other two models. The noticeable difference between the two linear elastic and hyperelastic models is not observed in calculating the average OSI.

High OSI values can cause regions of the arterial wall to experience bidirectional shear stress, leading to the activation of mechanosensitive signaling pathways within the endothelial cells. This activation can cause the production of inflammatory cytokines, growth factors, and enzymes that further weaken the arterial wall and contribute to aneurysm growth and rupture [65]. In particular, high OSI values can activate nuclear factor kappa B (NF-kB) in endothelial cells, leading to the production of pro-inflammatory cytokines and adhesion molecules, which promote inflammation and contribute to the growth and rupture of aneurysms [62, 66]. Furthermore, high OSI values can cause changes in the distribution and organization of the extracellular matrix (ECM) within the arterial wall. The shear stress associated with high OSI values can cause mechanical strain on the arterial wall, leading to the degradation of collagen and elastin fibers, which are responsible for maintaining the structural integrity of the arterial wall. The degradation of these fibers can lead to a loss of structural support and an increased susceptibility to aneurysm formation and rupture

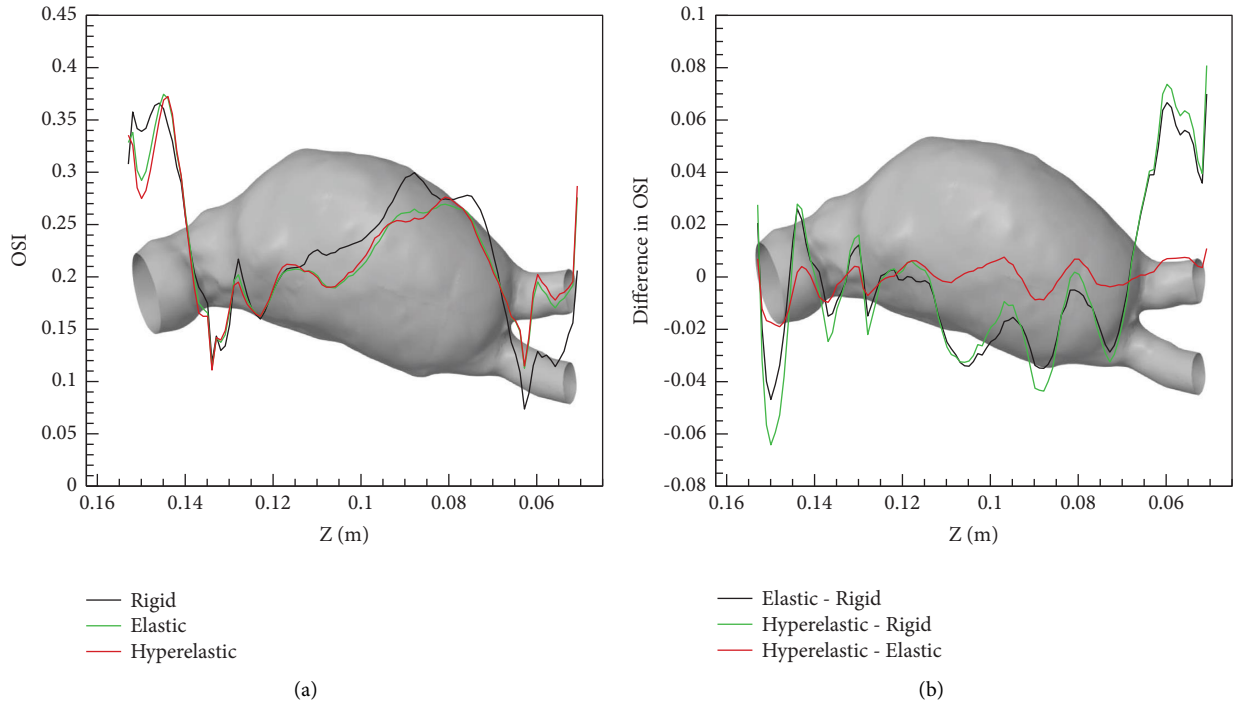

Figure 17: Comparison of different models in predicting average OSI along z direction; (a) average OSI for each model; (b) difference in models' predictions.

[67]. Based on Figures 15 and 16, it can be found that the area most affected by high oscillatory shear indices (OSIs) is at the end of the lumen and before the bifurcation. Considering the previously mentioned decrease in shear stress in this area, it can be concluded that the risk of thrombus formation is high. Other areas also show points with high OSI, which cannot be equated with a high risk of thrombus formation in these areas due to high shear stress. Linear elastic and hyperelastic models show similar results in terms of OSI, similar to shear stress. Interestingly, despite the analysis of shear stress, the rigid model predicts a higher risk of thrombus formation than the other two models based on the analysis of OSI values. Therefore, it cannot be conclusively determined which model is pessimistic or optimistic, and it is necessary to examine other hemodynamic parameters, such as RRT.

3.5. Relative Residence Time (RRT). In Figure 18, the predicted values of RRT by all three models used for the aneurysmal wall are shown. Unlike OSI, the points with high RRT values are only observed in one region, which is located in the lower part of the sac. The TAWSS values in this region are very low, and the OSI values are very high; therefore, the high RRT values, which have a direct relationship with OSI and an inverse relationship with TAWSS, are justifiable. The rigid model predicts a wider region for high RRT values, while in the linear elastic and hyperelastic models, points with high RRT values are concentrated in two small regions. This difference in the prediction of the RRT parameter by the models used is more apparent in Figure 19. By looking at this figure, it can be concluded that the difference between the linear elastic and hyperelastic models is very small and only related to the maximum RRT region.

From Figures 18 and 19, it is not possible to determine which model predicts a higher or lower level of RRT. To better understand this issue, Figure 20 is useful. By examining Figure 20, which shows the average RRT values along the Z-axis, it can be concluded that in a wide region of the aneurysm location under the influence, the hyperelastic model evaluates the RRT value higher than the other two models, although the predicted values by the linear elastic model are close to those of the hyperelastic model. However, it should be noted that the rigid model has predicted a higher value for this parameter at the maximum RRT location compared to the other two models.

The duration for which particles remain attached to the wall is directly related to the combined effect of OSI and TAWSS, which also has a significant connection to the biological processes of blood clotting [68]. Increased levels of OSI often indicate low TAWSS, and both of these factors serve as indicators of vascular damage [69]. However, it should be noted that regions with high OSI values may not always correspond to regions with low TAWSS values [61]. In studies that examine blood flow patterns, RRT is a reliable measure used to identify areas where there is low wall shear stress and high oscillation [70]. The regions of the aorta that are affected by aneurysmal dilation have notably higher RRT than the non-dilated regions. This positive correlation between RRT and aneurysm growth rate suggests that elevated RRT levels may indicate lower wall shear stress and higher oscillating

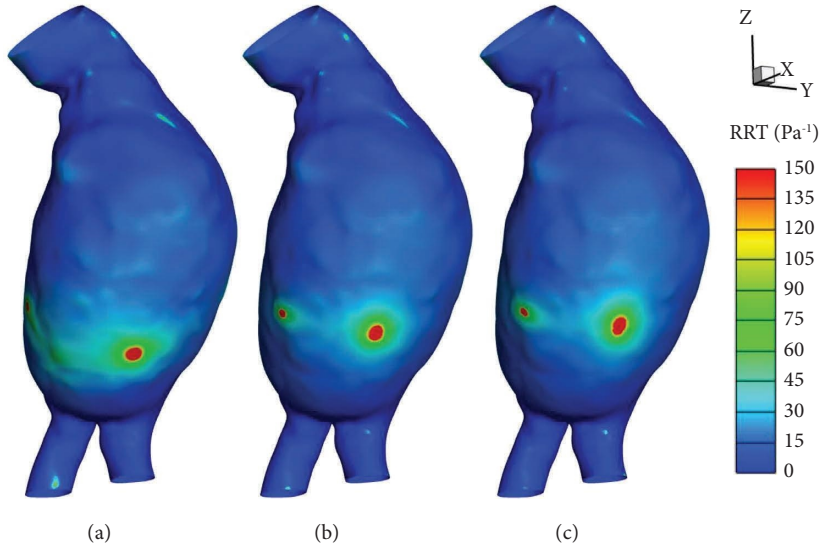

FIGURE 18: RRT contours on the aortic wall for different models: (a) rigid wall model; (b) linear elastic wall model; (c) hyperelastic wall model.

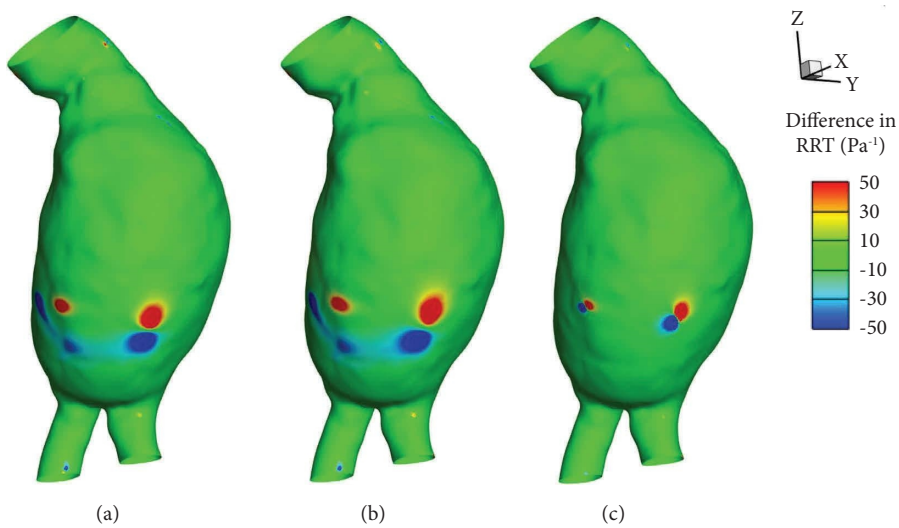

FIGURE 19: Difference in RRT contours on the aortic wall between different models; (a) $RRT_{elastic}$ - RRT_{rigid}; (b) $RRT_{hyperelastic}$ - RRT_{rigid}; (c) $RRT_{hyperelastic}$ - $RRT_{elastic}$.

shear stress, both of which can contribute to the development and progression of an aneurysm. [71]. As can be seen in Figures 18 to 20, in all three models, the RRT value is higher at two points in the lower half of the expanded region, and as a result, the probability of thrombus formation is much higher at these points than at other points. In contrast to what was observed in the analysis of TAWSS and high OSI values, a smaller region of the aneurysmal aorta is susceptible to thrombus formation. As expected, linear elastic and hyperelastic models predict similar values for the RRT parameter, but the situation is somewhat different for the rigid model. Generally, elastic models predict higher RRT values in a wide region of the aorta than the rigid model, but it is the rigid model that considers a higher risk of thrombus formation at critical points. Furthermore, the distance between critical points in the rigid model is greater than in the two elastic models. This issue is rooted in the absence of differentiation in this model, which heavily influences other hemodynamic parameters that are dependent on the shear stress, which is itself dependent on the differentiation of the aortic wall. Accurate knowledge of the amount and location of critical points is essential for clinical studies, and therefore, caution must be exercised when using the rigid model.

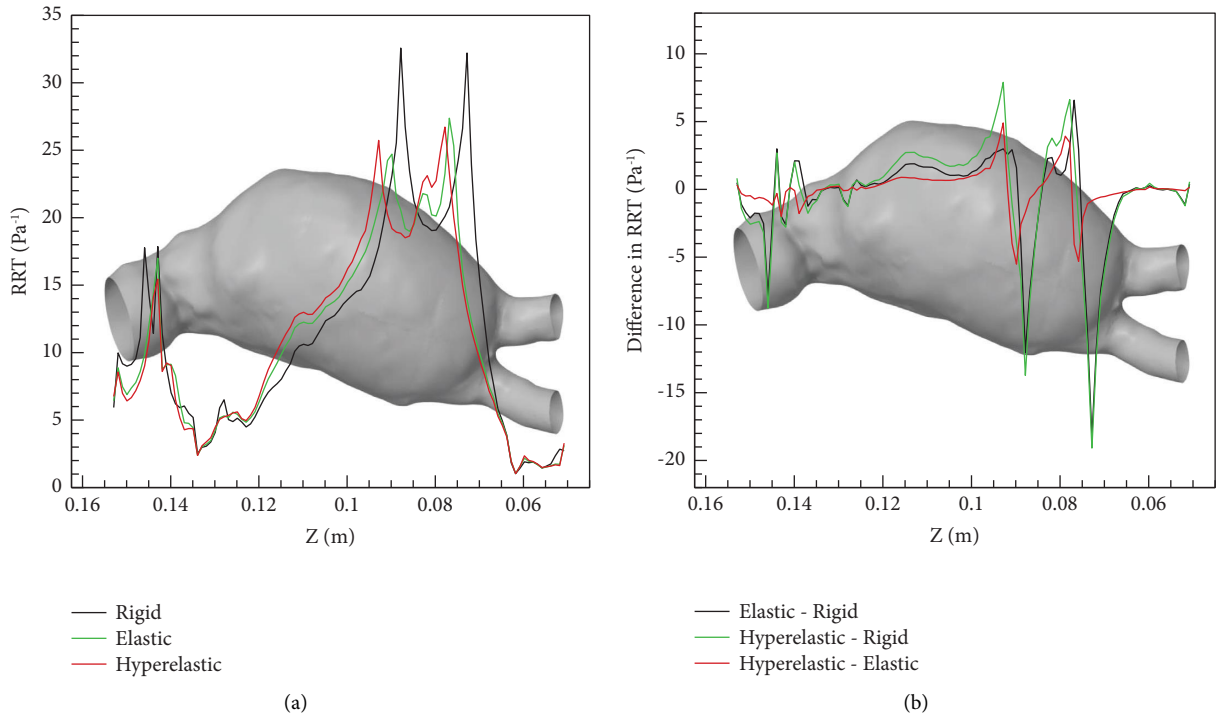

FIGURE 20: Comparison of different models in predicting average RRT along z direction; (a) average RRT for each model; (b) difference in models' predictions.

4. Conclusions

The employment of linear elastic and rigid wall models is prevalent in the numerical simulation of abdominal aortic aneurysms, yet their accuracy remains underexplored. This investigation delineates the distinctions between these conventional models and the more complex, realistic hyperelastic models. Findings indicate that while linear elastic models align closely with hyperelastic models in terms of evaluated results, this concordance diminishes when compared to the rigid model.

Notably, hyperelastic models predict slightly higher strain differentials and assess von Mises stress within the wall more extensively than linear elastic models, suggesting a more conservative estimation regarding rupture risk by the latter, albeit by a marginal difference. In regions subjected to high shear stress, rigid models estimate lower time-averaged wall shear stress (TAWSS) than their counterparts, implying a diminished thrombosis risk assessment under conditions of extreme shear. Conversely, hyperelastic models forecast higher shear stress levels in these areas than linear elastic models, although the variance is minimal. Under the aneurysm, where shear stress is notably low, rigid models predict higher TAWSS values than both linear elastic and hyperelastic models, with linear elastic models showing substantial agreement with hyperelastic outcomes. Despite the rigid model's higher shear stress oscillations in this region, analysis of the relative residence time (RRT) parameter reveals a lower thrombosis risk prediction across a broad segment of the aortic wall, in comparison with the alternative models. The linear elastic model also suggests a reduced thrombosis risk here, relative to hyperelastic models, but the difference is not markedly significant.

Considering hyperelastic models as a benchmark, the accuracy of linear elastic models in forecasting aortic rupture and thrombosis formation risk appears reasonable. However, caution is advised with the rigid model's application. The findings substantiate the linear elastic model's applicability within certain scenarios, simultaneously emphasizing the imperative for hyperelastic models to achieve a deeper, more nuanced comprehension of AAA dynamics. Through methodical model comparison, this investigation contributes substantially to theoretical knowledge and bears profound clinical practice implications, particularly in refining the precision of rupture and thrombosis risk evaluations. Addressing a critical research gap, the study advocates for the progressive embrace of advanced modeling techniques in AAA analysis, spotlighting their importance in both future research and enhanced clinical outcomes.

5. Limitations

This study critically assessed the accuracy of simplified wall models (rigid and linear elastic) versus the hyperelastic model in predicting AAA rupture and thrombosis risk. While simplified models are favored for their computational efficiency, they inherently lack the fidelity to fully represent the aortic wall's biomechanics. The hyperelastic model, despite its closer approximation to the true mechanical behavior of arterial walls, also presents limitations primarily

due to the reliance on literature-based material parameters. These parameters, while informed by existing studies, may not fully encapsulate the individual variability present in human tissues, possibly affecting the model's precision in predicting rupture and thrombosis risk.

Additionally, the study's boundary conditions were derived from literature data rather than patient-specific clinical measurements. This approach, while necessary in the absence of accessible patient data, introduces a degree of generalization that may not accurately reflect the unique physiological conditions of individual patients. Such generalizations could limit the model's applicability for predicting patient-specific outcomes.

Despite these limitations, this study provides valuable insights into the comparative accuracy of simplified and hyperelastic models in predicting key hemodynamic parameters relevant to the assessment of rupture and thrombosis risk in AAAs. By highlighting the trade-offs between model complexity and computational efficiency, it contributes to the ongoing discourse on optimizing AAA modeling approaches for both research and clinical applications.

Data Availability

The data used to support the findings of this study are available from the corresponding author upon request.

Conflicts of Interest

The author declares that there are no conflicts of interest related to this research.

Acknowledgments

The author thanks Embodi3D website (https://www.embodi3d.com) for providing the CT scan data, which served as the foundation for the geometric preparations. The author also wishes to express thanks to ChatGPT, whose assistance was invaluable in polishing the text to enhance the manuscript's clarity and readability.

References

[1] J. D. Humphrey, "Coupling haemodynamics with vascular wall mechanics and mechanobiology to understand intracranial aneurysms," *International Journal of Computational Fluid Dynamics*, vol. 23, no. 8, pp. 569–581, 2009.

[2] R. Valente, A. Mourato, M. Brito, J. Xavier, A. Tomás, and S. Avril, "Fluid–structure interaction modeling of ascending thoracic aortic aneurysms in simvascular," *Biomechanics*, vol. 2, no. 2, pp. 189–204, 2022.

[3] R. Jayendiran, B. Nour, and A. Ruimi, "Computational analysis of Nitinol stent-graft for endovascular aortic repair (EVAR) of abdominal aortic aneurysm (AAA): crimping, sealing and fluid-structure interaction (FSI)," *International Journal of Cardiology*, vol. 304, pp. 164–171, 2020.

[4] D. Zschäpitz, B. Bohmann, B. Lutz et al., "Rupture risk parameters upon biomechanical analysis independently change from vessel geometry during abdominal aortic aneurysm growth," *JVS-Vascular Science*, vol. 4, Article ID 100093, 2023.

[5] J. D. Humphrey and G. A. Holzapfel, "Mechanics, mechanobiology, and modeling of human abdominal aorta and aneurysms," *Journal of Biomechanics*, vol. 45, no. 5, pp. 805–814, 2012.

[6] M. Gonzalez-Urquijo, R. G. de Zamacona, A. K. M. Mendoza et al., "3D modeling of blood flow in simulated abdominal aortic aneurysm," *Vascular and Endovascular Surgery*, vol. 55, no. 7, pp. 677–683, 2021.

[7] J. Moradicheghamahi, M. Qasim, S. Jafarpour, and H. Farokhi, "Investigation of the effects of an inferior vena cava filter and captured clot size on the hemodynamic parameters in non-Newtonian turbulent pulsatile blood flow," *Applied Bionics and Biomechanics*, vol. 2023, Article ID 2439775, 18 pages, 2023.

[8] J. Moradicheghamahi, G. Fortuny, J. M. López, D. Puigjaner, J. Herrero, and Y. Azeli, "The effect of thoracic dimensions on compression depth during cardiopulmonary resuscitation," *International Journal for Numerical Methods in Biomedical Engineering*, vol. 39, no. 7, p. 3718, 2023.

[9] J. Moradicheghamahi, G. Fortuny, J. M. López, J. Herrero, and D. Puigjaner, "Deformation of the myocardium during CPR," 2022, https://arxiv.org/abs/2205.15804.

[10] F. Mezali, S. Benmamar, K. Naima, H. Ameur, and O. Rafik, "Evaluation of stent effect and thrombosis generation with different blood rheology on an intracranial aneurysm by the Lattice Boltzmann method," *Computer Methods and Programs in Biomedicine*, vol. 219, Article ID 106757, 2022.

[11] F. Mezali, K. Naima, S. Benmamar, and A. Liazid, "Study and modeling of the thrombosis of small cerebral aneurysms, with and without flow diverter, by the lattice Boltzmann method," *Computer Methods and Programs in Biomedicine*, vol. 233, Article ID 107456, 2023.

[12] K. Kanokjaruvijit, T. Donprai-On, N. Phanthura, P. Noidet, and J. Siripokharattana, "Wall shear stress and velocity distributions in different types of stenotic bifurcations," *Journal of Mechanical Science and Technology*, vol. 31, no. 5, pp. 2339–2349, 2017.

[13] J. Moradicheghamahi, J. Sadeghiseraji, and M. Jahangiri, "Numerical solution of the Pulsatile, non-Newtonian and turbulent blood flow in a patient specific elastic carotid artery," *International Journal of Mechanical Sciences*, vol. 150, pp. 393–403, 2019.

[14] A. Chen, A. A. B. Basri, N. B. Ismail, M. Tamagawa, D. Zhu, and K. A. Ahmad, "Simulation of mechanical heart valve dysfunction and the non-Newtonian blood model approach," *Applied Bionics and Biomechanics*, vol. 2022, Article ID 9612296, 14 pages, 2022.

[15] S. Kumar, B. Kumar, and S. Rai, "Influence of abdominal aortic aneurysm shape on hemodynamics in human aorto-femoral arteries: a transient open-loop study," *Physics of Fluids*, vol. 35, no. 4, 2023.

[16] N. T. Philip, B. S. V. Patnaik, and S B J, "Fluid structure interaction study in model abdominal aortic aneurysms: influence of shape and wall motion," *International Journal for Numerical Methods in Biomedical Engineering*, vol. 37, no. 3, p. 3426, 2021.

[17] H. Yi, Z. Yang, M. Johnson, L. Bramlage, and B. Ludwig, "Hemodynamic characteristics in a cerebral aneurysm model using non-Newtonian blood analogues," *Physics of Fluids*, vol. 34, no. 10, Article ID 103101, 2022.

[18] S. Bhushan, D. K. Walters, and G. W. Burgreen, "Laminar, turbulent, and transitional simulations in benchmark cases with cardiovascular device features," *Cardiovascular Engineering and Technology*, vol. 4, no. 4, pp. 408–426, 2013.

[19] M. R. Borse, *Turbulent Simulations of Feline Aortic Flow under Hypertrophic Cardiomyopathy Heart Condition*, Mississippi State University, Starkville, MS, USA, 2016.

[20] J. Moradicheghamahi, M. Jahangiri, M. Mousaviraad, and M. R. Sadeghi, "Computational studies of comparative and cumulative effects of turbulence, fluid–structure interactions, and uniform magnetic fields on pulsatile non-Newtonian flow in a patient-specific carotid artery," *Journal of the Brazilian Society of Mechanical Sciences and Engineering*, vol. 42, no. 10, pp. 518–522, 2020.

[21] C. M. Prado, S. G. Ramos, J. Elias, and M. A. Rossi, "Turbulent blood flow plays an essential localizing role in the development of atherosclerotic lesions in experimentally induced hypercholesterolaemia in rats," *International Journal of Experimental Pathology*, vol. 89, no. 1, pp. 72–80, 2008.

[22] M. Jahangiri, M. Saghafian, and M. R. Sadeghi, "Numerical study of turbulent pulsatile blood flow through stenosed artery using fluid-solid interaction," *Computational and Mathematical Methods in Medicine*, vol. 2015, Article ID 515613, 10 pages, 2015.

[23] P. D. Stein and H. N. Sabbah, "Measured turbulence and its effect on thrombus formation," *Circulation Research*, vol. 35, no. 4, pp. 608–614, 1974.

[24] S. Murali Krishna, S. K. Morton, J. Li, and J. Golledge, "Risk factors and mouse models of abdominal aortic aneurysm rupture," *International Journal of Molecular Sciences*, vol. 21, no. 19, p. 7250, 2020.

[25] S. S. Raut, S. Chandra, J. Shum, and E. A. Finol, "The role of geometric and biomechanical factors in abdominal aortic aneurysm rupture risk assessment," *Annals of Biomedical Engineering*, vol. 41, no. 7, pp. 1459–1477, 2013.

[26] V. Kessler, J. Klopf, W. Eilenberg, C. Neumayer, and C. Brostjan, "AAA revisited: a comprehensive review of risk factors, management, and hallmarks of pathogenesis," *Biomedicines*, vol. 10, no. 1, p. 94, 2022.

[27] C. Trenti, M. Ziegler, N. BjarnegÃ¥rd, T. Ebbers, M. Lindenberger, and P. Dyverfeldt, "Wall shear stress and relative residence time as potential risk factors for abdominal aortic aneurysms in males: a 4D flow cardiovascular magnetic resonance caseâ€ "control study," *Journal of Cardiovascular Magnetic Resonance*, vol. 24, no. 1, p. 18, 2022.

[28] F. Nieto-Palomo, M.-A. Perez-Rueda, L.-M. Lipsa et al., "Statistical techniques for predicting rupture risk in abdominal aortic aneurysms: a contribution based on bootstrap," *Science Progress*, vol. 104, no. 2, Article ID 00368504211003785, 2021.

[29] S. Polzer and T. C. Gasser, "Biomechanical rupture risk assessment of abdominal aortic aneurysms based on a novel probabilistic rupture risk index," *Journal of The Royal Society Interface*, vol. 12, no. 113, Article ID 20150852, 2015.

[30] B. Teng, Z. Zhou, Y. Zhao, and Z. Wang, "Combined curvature and wall shear stress analysis of abdominal aortic aneurysm: an analysis of rupture risk factors," *Cardiovascular and Interventional Radiology*, vol. 45, no. 6, pp. 752–760, 2022.

[31] S. N. S. H. Chittajallu, A. Richhariya, K. M. Tse, and V. Chinthapenta, "A review on damage and rupture modelling for soft tissues," *Bioengineering*, vol. 9, no. 1, p. 26, 2022.

[32] S. de Gelidi and A. Bucchi, "Comparative finite element modelling of aneurysm formation and physiologic inflation in the descending aorta," *Computer Methods in Biomechanics and Biomedical Engineering*, vol. 22, no. 15, pp. 1197–1208, 2019.

[33] H. Dehghani, *Mechanical modeling of poroelastic and residually stressed hyperelastic materials and its application to biological tissues*, Thesis for: Ph.D, Advisor: Prof. Jose Merodio, Menlo Park, CA, USA, 2019.

[34] A. Mantha, "Hemodynamic analysis of flow near cerebral aneurysms: insight into aneurysm formation and effects of intervention," 2012, https://uh-ir.tdl.org/items/12a202fe-3055-47ab-8539-1973236338bd.

[35] Y. Zhu, "Computational analysis of the hemodynamic performance of novel endovascular and surgical procedures for complex aortic diseases," 2020, https://core.ac.uk/download/pdf/511316843.pdf.

[36] C. Reeps, M. Gee, A. Maier, M. Gurdan, H.-H. Eckstein, and W. A. Wall, "The impact of model assumptions on results of computational mechanics in abdominal aortic aneurysm," *Journal of Vascular Surgery*, vol. 51, no. 3, pp. 679–688, 2010.

[37] A. Fluent, *16.2: Fluent Theory Guide*, ANSYS Help Viewer, France, Europe.

[38] J. Sadeghiseraji, J. Moradicheghamahi, and A. Sedaghatkish, "Investigation of a vortex tube using three different RANS-based turbulence models," *Journal of Thermal Analysis and Calorimetry*, vol. 143, no. 6, pp. 4039–4056, 2021.

[39] M. Jahangiri, M. Saghafian, and M. R. Sadeghi, "Numerical simulation of hemodynamic parameters of turbulent and pulsatile blood flow in flexible artery with single and double stenoses," *Journal of Mechanical Science and Technology*, vol. 29, no. 8, pp. 3549–3560, 2015.

[40] J. Biasetti, T. C. Gasser, M. Auer, U. Hedin, and F. Labruto, "Hemodynamics of the normal aorta compared to fusiform and saccular abdominal aortic aneurysms with emphasis on a potential thrombus formation mechanism," *Annals of Biomedical Engineering*, vol. 38, no. 2, pp. 380–390, 2010.

[41] C. Mills, I. Gabe, J. Gault et al., "Pressure-flow relationships and vascular impedance in man," *Cardiovascular Research*, vol. 4, no. 4, pp. 405–417, 1970.

[42] M. Jahangiri, M. Saghafian, and M. Sadeghi, "Numerical study of hemodynamic parameters in pulsatile turbulent blood flow in flexible artery with stenosis," in *The 22st Annual International Conference on Mechanical Engineering-Isme2014*, Shahid Chamran University, Ahvaz, Iran, 2014.

[43] M. Jahangiri, M. Saghafian, and M. Sadeghi, "Effects of non-Newtonian behavior of blood on wall shear stress in an elastic vessel with simple and consecutive stenosis," *Biomedical and Pharmacology Journal*, vol. 8, no. 1, pp. 123–131, 2015.

[44] D. Wang, F. Serracino-Inglott, and J. Feng, "Numerical simulations of patient-specific models with multiple plaques in human peripheral artery: a fluid-structure interaction analysis," *Biomechanics and Modeling in Mechanobiology*, vol. 20, no. 1, pp. 255–265, 2021.

[45] M. Raghavan and D. A. Vorp, "Toward a biomechanical tool to evaluate rupture potential of abdominal aortic aneurysm: identification of a finite strain constitutive model and evaluation of its applicability," *Journal of Biomechanics*, vol. 33, no. 4, pp. 475–482, 2000.

[46] N. T. Philip, B. S. V. Patnaik, and B. J. Sudhir, "Hemodynamic simulation of abdominal aortic aneurysm on idealised models: investigation of stress parameters during disease progression," *Computer Methods and Programs in Biomedicine*, vol. 213, Article ID 106508, 2022.

[47] M. Girfoglio, F. Ballarin, G. Infantino et al., "Non-intrusive PODI-ROM for patient-specific aortic blood flow in presence of a LVAD device," *Medical Engineering & Physics*, vol. 107, Article ID 103849, 2022.

[48] G. Hyde-Linaker, P. H. Barrientos, S. Stoumpos, D. B. Kingsmore, and A. Kazakidi, "Patient-specific computational haemodynamics associated with the surgical

creation of an arteriovenous fistula," *Medical Engineering & Physics*, vol. 105, Article ID 103814, 2022.

[49] M. Jahangiri, M. Saghafian, and M. R. Sadeghi, "Numerical simulation of non-Newtonian models effect on hemodynamic factors of pulsatile blood flow in elastic stenosed artery," *Journal of Mechanical Science and Technology*, vol. 31, no. 2, pp. 1003–1013, 2017.

[50] J. Urevc, I. Žun, M. Brumen, and B. Štok, "Modeling the effect of red blood cells deformability on blood flow conditions in human carotid artery bifurcation," *Journal of Biomechanical Engineering*, vol. 139, no. 1, Article ID 011011, 2017.

[51] H. Aryan, B. Beigzadeh, and M. Siavashi, "Euler-Lagrange numerical simulation of improved magnetic drug delivery in a three-dimensional CT-based carotid artery bifurcation," *Computer Methods and Programs in Biomedicine*, vol. 219, Article ID 106778, 2022.

[52] L. Wei, J. Wang, Q. Chen, and Z. Li, "Impact of stent malapposition on intracoronary flow dynamics: an optical coherence tomography-based patient-specific study," *Medical Engineering & Physics*, vol. 94, pp. 26–32, 2021.

[53] K. Capellini, E. Gasparotti, U. Cella et al., "A novel formulation for the study of the ascending aortic fluid dynamics with in vivo data," *Medical Engineering & Physics*, vol. 91, pp. 68–78, 2021.

[54] S.-W. Lee, L. Antiga, and D. A. Steinman, "Correlations among indicators of disturbed flow at the normal carotid bifurcation," *Journal of Biomechanical Engineering*, vol. 131, no. 6, Article ID 61013, 2009.

[55] Y. Qiao, L. Mao, Y. Wang et al., "Hemodynamic effects of stent-graft introducer sheath during thoracic endovascular aortic repair," *Biomechanics and Modeling in Mechanobiology*, vol. 21, no. 2, pp. 419–431, 2022.

[56] L. Boussel, V. Rayz, C. McCulloch et al., "Aneurysm growth occurs at region of low wall shear stress: patient-specific correlation of hemodynamics and growth in a longitudinal study," *Stroke*, vol. 39, no. 11, pp. 2997–3002, 2008.

[57] M. Farsad, S. Zeinali-Davarani, J. Choi, and S. Baek, "Computational growth and remodeling of abdominal aortic aneurysms constrained by the spine," *Journal of Biomechanical Engineering*, vol. 137, no. 9, 2015.

[58] J. J. Hathcock, "Flow effects on coagulation and thrombosis," *Arteriosclerosis, Thrombosis, and Vascular Biology*, vol. 26, no. 8, pp. 1729–1737, 2006.

[59] E. DeRoo, A. Stranz, H. Yang, M. Hsieh, C. Se, and T. Zhou, "Endothelial dysfunction in the pathogenesis of abdominal aortic aneurysm," *Biomolecules*, vol. 12, no. 4, p. 509, 2022.

[60] K. B. Hansen and S. C. Shadden, "A reduced-dimensional model for near-wall transport in cardiovascular flows," *Biomechanics and Modeling in Mechanobiology*, vol. 15, no. 3, pp. 713–722, 2016.

[61] Z. Chen, H. Yu, Y. Shi et al., "Vascular remodelling relates to an elevated oscillatory shear index and relative residence time in spontaneously hypertensive rats," *Scientific Reports*, vol. 7, no. 1, pp. 2007–2010, 2017.

[62] S. Morel, S. Schilling, M. R. Diagbouga et al., "Effects of low and high aneurysmal wall shear stress on endothelial cell behavior: differences and similarities," *Frontiers in Physiology*, vol. 12, Article ID 727338, 2021.

[63] K. Sunderland, C. Haferman, G. Chintalapani, and J. Jiang, "Vortex analysis of intra-aneurismal flow in cerebral aneurysms," *Computational and Mathematical Methods in Medicine*, vol. 2016, Article ID 7406215, 16 pages, 2016.

[64] H. Wang, D. Balzani, V. Vedula, K. Uhlmann, and F. Varnik, "On the potential self-amplification of aneurysms due to tissue degradation and blood flow revealed from FSI simulations," *Frontiers in Physiology*, vol. 12, Article ID 785780, 2021.

[65] M. Ohta, N. Sakamoto, K. Funamoto, Z. Wang, Y. Kojima, and H. Anzai, "A review of functional analysis of endothelial cells in flow chambers," *Journal of Functional Biomaterials*, vol. 13, no. 3, p. 92, 2022.

[66] D. C. Baeriswyl, I. Prionisti, T. Peach et al., "Disturbed flow induces a sustained, stochastic NF-κB activation which may support intracranial aneurysm growth in vivo," *Scientific Reports*, vol. 9, no. 1, p. 4738, 2019.

[67] S. S. Veeturi, T. R. Patel, A. A. Baig et al., "Hemodynamic analysis shows high wall shear stress is associated with intraoperatively observed thin wall regions of intracranial aneurysms," *Journal of Cardiovascular Development and Disease*, vol. 9, no. 12, p. 424, 2022.

[68] H. A. Himburg, D. M. Grzybowski, A. L. Hazel, J. A. LaMack, X.-M. Li, and M. H. Friedman, "Spatial comparison between wall shear stress measures and porcine arterial endothelial permeability," *American Journal of Physiology- Heart and Circulatory Physiology*, vol. 286, no. 5, 2004.

[69] K. P. Papadopoulos, M. Gavaises, I. Pantos, D. G. Katritsis, and N. Mitroglou, "Derivation of flow related risk indices for stenosed left anterior descending coronary arteries with the use of computer simulations," *Medical Engineering & Physics*, vol. 38, no. 9, pp. 929–939, 2016.

[70] S.-W. Lee, L. Antiga, and D. A. Steinman, "Correlations among indicators of disturbed flow at the normal carotid bifurcation," *Journal of Biomechanical Engineering*, vol. 131, no. 6, Article ID 61013, 2009.

[71] G. J. J. Riccardello, D. N. Shastri, A. R. Changa et al., "Influence of relative residence time on side-wall aneurysm inception," *Neurosurgery*, vol. 83, no. 3, pp. 574–581, 2018.